de Haas–van Alphen Effect and Electronic Band Structure of Nickel†‡

D. C. Tsui*
Department of Physics and the James Franck Institute, University of Chicago, Chicago, Illinois
(Received 1 June 1967)

We present here a de Haas–van Alphen (DHVA) investigation of nickel utilizing low-frequency field-modulation techniques in magnetic fields extending to 38 kG and at temperatures down to 0.3°K. Two distinct sets of DHVA-frequency branches were obtained with the magnetic field in either the $(1\bar{1}0)$ or the (100) crystallographic symmetry plane. The assignment of these to sheets of the nickel Fermi surface is discussed in terms of the general features of band-structure models recently proposed for ferromagnetic nickel. The low-frequency branches are assigned to the [111]-directed necks of the spin-$\uparrow$ s-band electron sheet. The high-frequency branches are shown to arise from a d-band hole pocket derived from a pure X_5 level in the spin-$\downarrow$ band. No evidence was obtained for d-band hole pockets derived from the $X_2\downarrow$ and $L_3\downarrow$ levels. Since the signal-to-noise ratio for detecting the high-frequency branches was large, the fact that we did not observe any DHVA oscillations assignable to either the $X_2\downarrow$ or $L_3\downarrow$ pockets makes their existence doubtful.

I. INTRODUCTION

FERROMAGNETISM in transition metals has long been an outstanding unsolved problem in physics. At present it still defies a complete theoretical understanding. Many models have been proposed to explain various aspects of the phenomena, but none provide a satisfactory description of the entire picture. The obvious fundamental reason for this is that we do not completely understand the behavior of electrons in these metals.[1]

The de Haas–van Alphen (DHVA) effect has proven in recent years to be one of the most powerful tools available for probing the behavior of conduction electrons in nonmagnetic metals.[2–4] It arises from the quantization of the conduction electrons's angular momentum about the magnetic induction **B** in the sample. Because of the sharp cutoff in the electron distribution at the Fermi energy E_F, this quantization can be observed experimentally as quantum oscillations in the magnetization of the sample when the magnetic induction **B** in the sample is varied. The DHVA part of the magnetization has the general form[5]

$$\mathbf{M}(B,\theta,\varphi,T)=\sum_i \boldsymbol{\alpha}_i(B,\theta,\varphi,T)\times\sin[2\pi F_i(\theta,\varphi)/B+\beta_i(\theta,\varphi)], \quad (1a)$$

$$\boldsymbol{\alpha}_i(B,\theta,\varphi,T)=\mathbf{C}_i(\theta,\varphi)B^{1/2}T[\sinh(2\pi^2kT/\hbar\omega_c)]^{-1}, \quad (1b)$$

where $\alpha_1(B,\theta,\varphi,T)$ and $\beta_i(\theta,\varphi)$ are the amplitude and phase, respectively, of the quantum oscillations of frequency $F_i(\theta,\varphi)$ for a given temperature T and magnetic induction B, with the direction of B given by the polar coordinates (θ,φ) with respect to the fundamental crystallographic axes. $\mathbf{C}_i(\theta,\varphi)$ is the vector quantity determined by the geometry of the Fermi surface in the immediate neighborhood of the extremal plane. This determines both the direction and magnitude of the quantum magnetization. The frequency $F_i(\theta,\varphi)$ is related to the ith extremal cross-sectional area $A_i(\theta,\varphi)$ of the Fermi surface in planes normal to **B** by the Onsager-Lifshitz expression[6]:

$$2\pi F_i(\theta,\varphi)=(\hbar c/e)A_i(\theta,\varphi). \quad (2)$$

The summation in Eq. (1a) is over all extremal cross sections for a given direction (θ,φ) of **B**. Therefore, in principle, one can precisely map out the Fermi surface of a metal by studying the field-orientation dependence of its DHVA frequencies. One can, in addition, obtain the effective cyclotron mass of the electrons on the Fermi surface by measuring the temperature dependence of the DHVA amplitude. This measured effective mass has to be corrected for many-body mass-enhancement effects to yield the one-electron band-structure mass[7]

$$m^*=(\hbar^2/2\pi)(dA/dE)\,|_{E=E_F}. \quad (3)$$

Though the knowledge of the Fermi-surface geometry of a metal allows one to determine its electronic band structure only in the vicinity of the Fermi level, it imposes stringent experimental restrictions which a valid band-structure calculation must meet. Since optical experiments which can in principle probe the band structure for energies other than E_F have not yielded reliable results for most metals, the Fermi-surface experiments offer the only direct means of obtaining information about the electronic band structure of the metal.

* General Electric Predoctoral Fellow. Present address: Bell Telephone Laboratories, Murray Hill, New Jersey.
This research was supported in part by the U.S. Army Research Office (Durham), the National Science Foundation, and the Advanced Research Projects Agency. The use of the facilities of the Low Temperature Laboratory, supported by the National Science Foundation, and the Materials Preparation Laboratory, supported by the Advanced Research Projects Agency, are gratefully acknowledged.

‡ Submitted in partial fulfillment of the requirements for the degree of Doctor of Philosophy at the University of Chicago.

[1] N. F. Mott, Advan. Phys. **13**, 325 (1964).
[2] N. W. Ashcroft, Phil. Mag. **8**, 2055 (1963).
[3] J. R. Anderson and A. V. Gold, Phys. Rev. **139**, A1459 (1965).
[4] J. C. Kimball, R. W. Stark, and F. M. Mueller (to be published).
[5] I. M. Lifshitz and A. M. Kosevich, Zh. Eksperim. i Teor. Fiz. **29**, 730 (1955) [English transl.: Soviet Phys.—JETP **2**, 636 (1956)].
[6] L. Onsager, Phil. Mag. **43**, 1006 (1952).
[7] S. Nakajima and M. Watabe, Progr. Theoret. Phys. (Kyoto) **30**, 772 (1963).

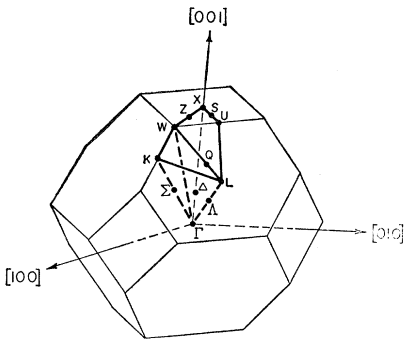

FIG. 1. The first Brillouin Zone for a fcc lattice. The major symmetry points and lines are designated according to the notation of Bouchaert, Smoluchowski, and Wigner.

Of the ferromagnetic transition metals, the DHVA effect was first observed in iron by Anderson and Gold[8] using pulsed-field techniques and in nickel by Joseph and Thorsen (JT)[9] using torsion-balance techniques. These earlier experiments showed that one can, in practice, use the DHVA effect as a tool to probe the electronic band structures of ferromagnetic metals. This paper describes an investigation of the DHVA effect in nickel utilizing low-frequency field-modulation techniques in external fields extending to 38 kG and temperatures down to 0.3°K. The results are discussed in the light of the general features of recently proposed models for ferromagnetic nickel band structure.

II. MODEL BAND STRUCTURE AND FERMI SURFACE FOR FERROMAGNETIC NICKEL

There have been a number of models proposed for the band structure of ferromagnetic nickel.[10–16] These are all based on the assumption that the ferromagnetic splitting is small in comparison with the crystal potential so that the ferromagnetic band structure can be obtained from the paramagnetic band structure[17–20] by treating the ferromagnetic splitting as a perturbation. The resulting model must yield the correct magneton number[21] and have Fermi-surface sheets enclosing a net volume corresponding to one electron per atom.[22] In addition, one sheet must be open, similar to the copper Fermi surface, to satisfy the magnetoresistance experiments of Fawcett and Reed[23] and the DHVA experiments of JT. The DHVA data which will be discussed in Sec. IV offer the first independent confirmation of this general approach to the ferromagnetic nickel band structure.

Ferromagnetic nickel has the fcc crystal structure. Its Brillouin zone (BZ) is shown in Fig. 1 together with the major symmetry points and lines which are designated according to the notation of Bouchaert, Smoluchowski, and Wigner. Figure 2 shows the paramagnetic nickel band structure obtained from Hanus's augmented-plane-wave (APW) calculation[17]; Fig. 3 shows a schematic ferromagnetic band structure obtained from this which is representative of the recently proposed models. We choose the convention that the majority electrons have spin-↑ and label the bands from 1 to 6 in order of increasing energy. Figure 4 shows, in the major symmetry planes, the cross sections of the Fermi surface predicted by this schematic band structure. The first five spin-↑ bands are all filled. The Fermi-surface sheet in the sixth spin-↑ band is a large electron surface multiply connected by necks along the [111] directions. The spin-↓ bands have two large closed electron sheets centered on Γ and three sets of small hole pockets, one centered on L and two on X.

Since the Fermi energy of these three sets of hole pockets is quite small (a few hundredths of a rydberg), their existence in this model is only tentative. First-principles band-structure calculations in paramagnetic nickel[17–20] have demonstrated that, although the structure of the d bands is not very sensitive to the effective one-electron potential, the position of the d bands relative to the s band is very sensitive to this potential. It is thus reasonable to assume that the flatness of the Z_2 d level is preserved in going into the ferromagnetic state. Since this flat band yields a very high density of states near E_F, the $X_5\downarrow$ level must be above E_F to preserve the proper magneton number. Thus, the $X_5\downarrow$ hole pocket must exist. On the other hand, the L_2' and L_3 levels are particularly sensitive to the one-electron effective potential. In fact, their ordering in energy could even be reversed from that shown in Fig. 2 by a small change in the potential.[16,18] If the ordering of the $L_2'\downarrow$ and the $L_3\downarrow$ levels is as shown in Fig. 3, an $L_3\downarrow$ pocket must exist for the same reason that the $X_5\downarrow$ pocket must exist. But, if the ordering is reversed, as shown in Fig. 5, the $L_2'\downarrow$ level is not necessarily above E_F. In case the $L_2'\downarrow$ is below E_F, there will be no hole pocket centered on L. Thus the existence of the $L_3\downarrow$ as well as the $X_2\downarrow$ pockets is not required by this model.

[8] J. R. Anderson and A. V. Gold, Phys. Rev. Letters **10**, 277 (1963).
[9] A. S. Joseph and A. C. Thorsen, Phys. Rev. Letters **11**, 554 (1963).
[10] H. Ehrenreich, H. R. Philipp, and D. J. Olechna, Phys. Rev. **131**, 2469 (1963).
[11] J. C. Phillips, Phys. Rev. **133**, A1020 (1964).
[12] S. Wakoh, J. Phys. Soc. Japan **20**, 1894 (1965).
[13] S. Wakoh and J. Yamashita, J. Phys. Soc. Japan **19**, 1342 (1964).
[14] L. Hodges and H. Ehrenreich, Phys. Letters **16**, 203 (1965).
[15] L. Hodges, H. Ehrenreich, and N. D. Lang, Phys. Rev. **152**, 505 (1966).
[16] J. W. D. Connolly, Phys. Rev. **159**, 415 (1967).
[17] J. G. Hannus, Massachusetts Institute of Technology, Solid State and Molecular Theory Group Quarterly Progress Report No. 44, 1962, p. 62 (unpublished).
[18] E. C. Snow, J. T. Waber, and A. C. Switendick, J. Appl. Phys. **37**, 1342 (1966).
[19] L. F. Mattheiss, Phys. Rev. **134**, A970 (1964).
[20] J. Yamashita, M. Fukuchi, and S. Wakoh, J. Phys. Soc. Japan **18**, 999 (1963).
[21] C. Kittel, *Introduction to Solid State Physics* (John Wiley & Sons, Inc., New York, 1956).
[22] E. Fawcett and W. A. Reed, Phys. Rev. **131**, 1463 (1963).
[23] E. Fawcett and W. A. Reed, Phys. Rev. Letters **9**, 336 (1962).

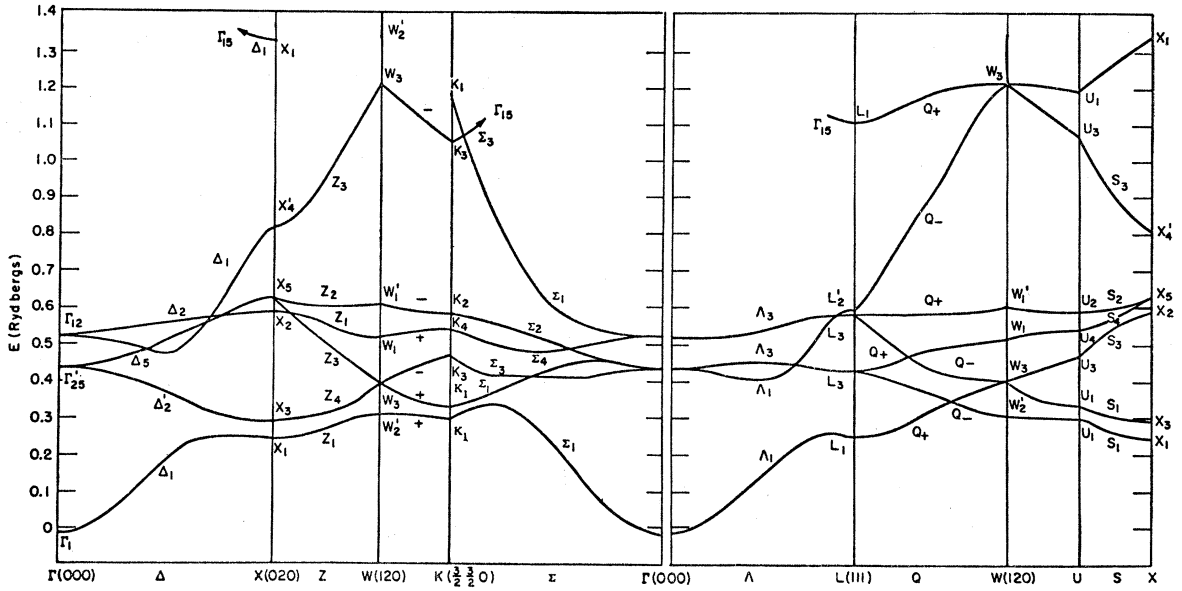

FIG. 2. Paramagnetic energy bands of nickel along main symmetry lines (taken from Ref. 17).

III. EXPERIMENTAL DETAILS

It is well known that in order to observe the DHVA effect in a sample, several experimental requirements must be satisfied.[24] First, the sample must be a single crystal of high purity and perfection. Second, the high magnetic field existing in the sample must have good uniformity. Third, the experiments must be carried out at low temperatures. These requirements, when applied to ferromagnetic transition metals, are very demanding. Consequently, there has been no detailed studies in any of these ferromagnetic metals. In the present DHVA investigation in nickel, we have attempted to overcome these difficulties.

A. Sample Preparation

The single-crystal samples used in this experiment were cut from a $\frac{3}{16}$-in.-diam rod which had been electron-beam zone-refined in high vacuum. A commercial electron-beam zone refiner was modified to yield vacuum in the 10^{-8}-mm-Hg range. The original high-purity polycrystalline nickel rod was obtained from Johnson, Matthey and Company. It was first etched in concentrated nitric acid to remove surface contamination and then annealed in atmosphere at 1000°C for 45 min. The resulting rod was coated with a layer of green nickel oxide. This was then zone-refined vertically downward with a sustained molten zone of about $\frac{1}{8}$ of an inch. During the first zone pass, decomposition of the nickel oxide was so violent that sparks were continually formed, and the resulting rod was rough in appearance. Additional zone passes were made until the resulting rod had a smooth and shiny appearance (the independent development of this technique is discussed by V. J. Albano and R. R. Soden[24a]).

The residual resistivity ratios (RRR) of the samples used in this experiment were not measured. However, the sample in which we first observed the neck frequency along the [111] direction at 30 kG had a RRR of about 3000. Since this same DHVA frequency was observed in fields as low as 2 kG in the higher-purity samples on which most of the data were taken, we assume that their RRR are somewhat higher. The Dingle scattering temperature for these samples was smaller than 0.5°K.

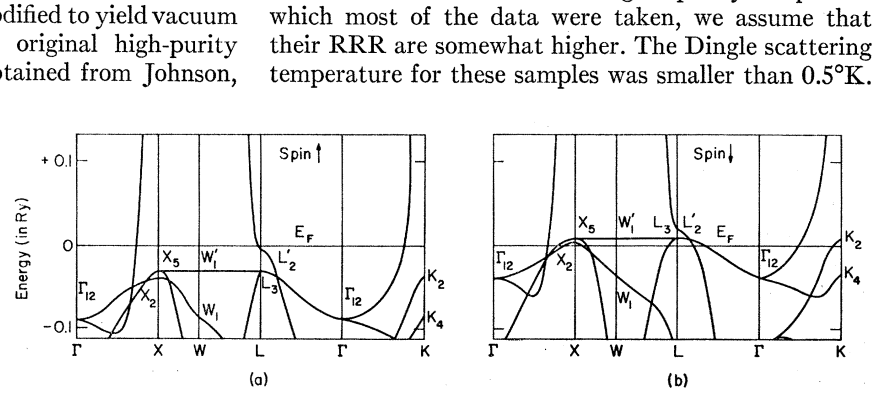

FIG. 3. Schematic band structure for ferromagnetic nickel. Spin up (↑) bands are assumed to have lower energy.

[24] C. Kittel, *Quantum Theory of Solids* (John Wiley & Sons, Inc., New York, 1963).
[24a] V. J. Albano and R. R. Soden, J. Electrochem. Soc. **113**, 511 (1966).

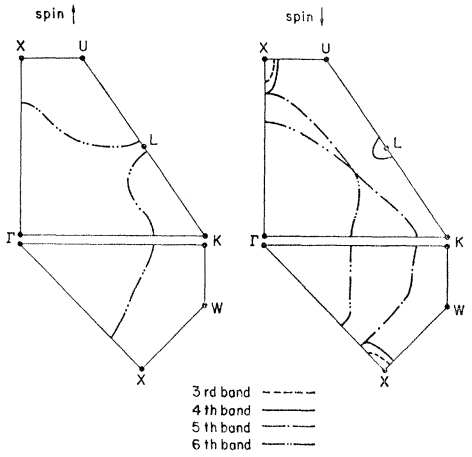

FIG. 4. Cross sections of the Fermi surface of nickel in major symmetry planes as predicted by the model band structure shown in Fig. 3. The bands are labeled from 1 to 6 in order of increasing energy.

We believe that the nickel oxide coating on the rod plays an essential role in this zone-refining purification process. The oxygen released from its decomposition during the refining process reduces the original carbon- and hydrogen-impurity contents of the rod and protects the molten zone from hydrocarbon contamination from the back-stream of the diffusion-pump oil used in our vacuum system. It also seems probable that the decomposition reaction of this nickel oxide coating causes precipitation of impurities inside the rod.

In ferromagnetic nickel, the magnetic induction **B** seen by the electrons participating in the DHVA effect is given by[21]

$$\mathbf{B}=\mathbf{H}+\mathbf{H}_D+4\pi\mathbf{M}(\mathbf{H}), \qquad (4)$$

where **H** is the applied external field, $\mathbf{H}_D$ is the demagnetization field due to the geometry of the sample, and **M** is the total magnetization of the sample. The homogeneity of the magnetic induction is obviously determined by that of **H**, **M**, and $\mathbf{H}_D$. Since only samples having ellipsoidal geometry can have a uniform demagnetization field $\mathbf{H}_D$, great care has been taken to prepare samples whose geometry approximated closely that of thin lens-shaped ellipsoids of revolution. Thin samples were chosen primarily to avoid skin-depth complications and to minimize eddy-current effects due to the field-modulation technique employed in detecting the DHVA signal.

The samples were first cut into circular disks 0.020 in. thick and 0.142 in. in diameter by using an Agietron spark cutter with a travelling wire attachment to minimize crystal damage. The sample disk normals were oriented along either a ⟨110⟩ or ⟨100⟩ crystallographic axis to within 0.5° by standard Laue back-reflection x-ray techniques. After being etched in concentrated nitric acid to remove surface contamination, the thin disks were electropolished in a solution of 5 parts concentrated H_2SO_4 and 2 parts water. The electropolished sample approximates closely a lens-shaped ellipsoid of revolution. This was then outgased at 1100°C for 1 h to remove interstitial impurities and strains.

B. He^3 Refrigerator

The preliminary results[25] of the present investigation indicated that for our sample at 1°K, thermal scattering was still the dominant line-broadening mechanism and that the DHVA signal from the heavy-mass *d*-band Fermi-surface sheets could be enhanced considerably by lowering the sample temperature. For this purpose, a simple He^3 refrigerator suitable for studying the DHVA effect using the low-frequency field-modulation techniques was constructed. Figure 6(a) shows a schematic drawing of the refrigerator together with the He^4 cryostat which provides its environment temperature of 1.15°K.

The whole system is designed to be used with an iron-core electromagnet with a $\frac{5}{8}$-in. gap. The He^4 cryostat was a stainless-steel design with interchangeable tails. The tail used in this experiment had an o.d. of 0.562 in. and an i.d. of 0.355 in. The double-wall He^3 Dewar had and o.d. of 0.335 in. and an i.d. of 0.293 in. The walls were made of 0.003-in.-thick type-321 stainless steel. The vacuum space between the concentric walls was sealed off at atmospheric pressure and room temperature. All of the electrical leads into the He^3 Dewar were heat-sunk at the transformer box by using superconducting lead strips epoxied to the wall of the box. The present system is capable of operating at 0.3°K. However, since liquid He^3 is a poor thermal conductor, the contents of the He^3 Dewar do not readily obtain thermal equilibrium. Consequently, it was impossible to accurately determine the temperature of the sample.

C. Detection Apparatus

The low-frequency field-modulation techniques employed in the present investigation were described in

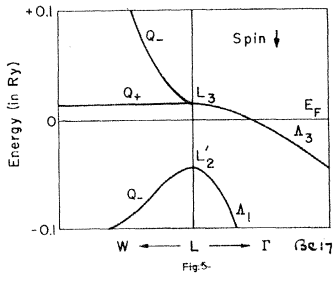

FIG. 5. An alternative ordering of energy levels (near E_f) about the symmetry point *L* (Ref. 16).

[25] D. C. Tsui and R. W. Stark, Phys. Rev. Letters **17**, 831 (1966).

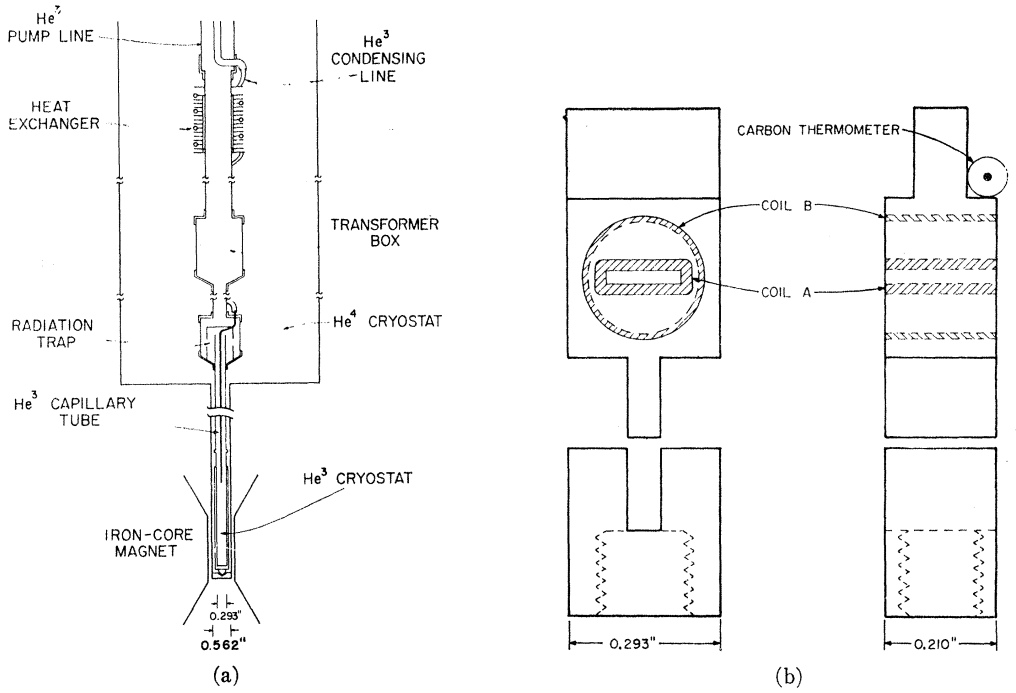

FIG. 6. Schematic drawings of (a) the He^3 system, and (b) the sample holder used in this experiment. The sample holder is mounted inside the liquid-He^3 bath.

detail by Stark and Windmiller.[26] We will mention only briefly what is pertinent to this discussion. The mathematics for the case of magnitude modulation used in this experiment are given in Appendix A.

The high dc magnetic field applied to the DHVA sample is modulated by an ac field, $H_m \cos\omega t$. The modulation frequency is low enough to avoid skin-depth complications. The amplitude H_m is usually larger than that normally used in a derivative-taking technique and is chosen according to the particular DHVA frequency to be detected. Because the DHVA magnetization is nonlinear in B, the induced emf in the pickup coil placed around the sample contains harmonics of the modulation frequency ω. The amplitude A_n of the nth harmonic has the form

$$A_n = \hat{\mu}\cdot\boldsymbol{\alpha}_i \sin[(2\pi F_i/B)+\beta_i+\tfrac{1}{2}(n\pi)]J_n(x),$$
$$x = 2\pi F_i H_m/B^2, \qquad (5)$$

where $J_n(x)$ is the Bessel function of the first kind of order n and $\hat{\mu}$ is a unit vector along the pickup coil axis. Phase-sensitive detection is then used to separate out the nth harmonic component of this induced emf. The amplitude of the DHVA oscillations of frequency F_i seen at the output of the phase-sensitive detector is proportional to the DHVA magnetization amplitude α_i multiplied by the Bessel-function factor $J_n(2\pi F_i H_m/B^2)$. For a given DHVA frequency F_i, the value of J_n is determined by the dc field strength and the modulation amplitude H_m. Thus, the value of H_m can be chosen to favor the detection of this particular frequency F_i.

In this experiment, the modulation frequency was kept below 100 Hz and the signal was detected at the second and the fourth harmonics. The modulation field was produced by a pair of Helmholtz coils mounted on the pole caps of the electromagnet. The pickup coil consists of coils A and B arranged in the sample holder as shown in Fig. 6(b). Since our sample has the shape of a thin disk, the pickup coil wound with 1500 turns of No. 50 gauge copper wire was made in the form of a thin rectangular parallelopiped having inside dimensions of 0.025 in.×0.140 in.×0.210 in. The sample was secured inside this coil by a thin layer of Dow Corning No. 200 fluid. The coil B was counterwound with 300 turns of copper wire on a spool 0.160 in. in diameter in order to buck out the emf induced directly in coil A by the modulation field. The pickup coil was balanced to within 0.3% when empty. With the sample mounted in place, the pickup coil becomes unbalanced because the flux due to the DHVA magnetization of the sample is more closely coupled to the flat coil A than to the bucking coil B. The unbalanced signal was fed to the primary of an impedance matching transformer, which is made of laminated core material from Allegheny Ludlum Steel Corporation and had a turns ratio of 100. The transformer box, which was surrounded by a superconducting lead shield, was part of the He^3 re-

[26] R. W. Stark and L. R. Windmiller (to be published).

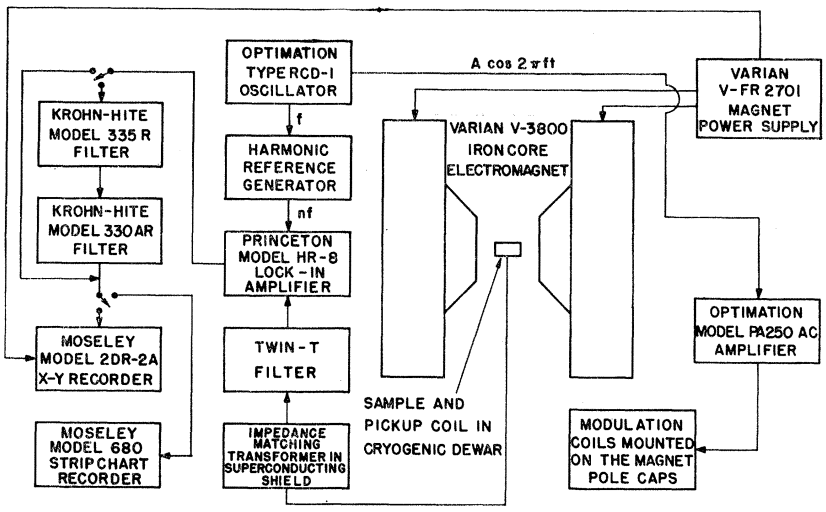

FIG. 7. Block diagram of the detection apparatus used in this experiment.

frigerator as shown in Fig. 6(a). The secondary of the transformer was fed into a passive twin-T filter tuned to reject the modulation frequency and the filter output was fed into a Princeton HR-8 phase-sensitive detector. The output of the detector was displayed either on the y axis of an x-y recorder or on a strip chart recorder. This detecting system, as diagrammed in Fig. 7, was capable of detecting signals as small as 10^{-10} V from the pickup coil.

D. Determining the B Field

The geometry of the samples used in this experiment approximates closely that of thin lens-shaped ellipsoids of revolution. The external field $\mathbf{H}$ is restricted to the equitorial plane of the sample. Since $\mathbf{M}(\mathbf{H})$ is saturated and directed along $\mathbf{H}$ for this geometry, the $\mathbf{B}$ field given by Eq. (4) is reduced to

$$\mathbf{B}=(H+H_{\text{In}})\hat{H}, \tag{6a}$$

$$H_{\text{In}}=(1-D)4\pi M_s, \tag{6b}$$

where D is the demagnetization factor for $\mathbf{H}$ along an axis in the sample plane, $4\pi M_s$ is the saturation magnetization of nickel at the sample temperature, and $\hat{H}$ is the unit vector along $\mathbf{H}$.

The applied field $\mathbf{H}$ was supplied by a 15-in. Varian electromagnet which can be rotated about its vertical axis at various uniform speeds. For fields below 15 kG, nuclear magnetic resonance (NMR) was used to calibrate the "fieldial" power supply to within 0.1%. Calibrations above 15 kG were obtained with a Rawson rotating probe which was accurate to better than 1%. The internal field H_{in}, given by Eq. (6b), is independent of the magnitude of H when $\mathbf{M}(\mathbf{H})$ is saturated. Thus it can be determined by utilizing the fact that the DHVA oscillations are periodic in B^{-1}.[8]

With $\mathbf{H}$ along the easy magnetization direction [111], sixty DHVA oscillations were observed as the field was swept from 12.600 to 6.955 kG. The value of H at the peak of each oscillation was measured accurately using NMR. H_{in} was then determined by fitting the peak number n and $(H+H_{\text{in}})^{-1}$ to a straight line by treating H_{in} as variable parameter and minimizing the root mean square deviation. Figure 8 shows the standard deviations of the slopes of the fitted lines versus the values of H_{in}. The value of H_{in}, determined from the best fit for the (110) sample (6.34±0.15 kG), was also used for the (100) sample which had the same geometry.

If the appropriate demagnetization factor D for an ellipsoid of revolution[27] equivalent to this sample is used, the saturation magnetization $4\pi M_s$, obtained from the internal field H_{in} determined above, is 6.7±0.2 kG. This value seems to be slightly larger than the previously measured value of 6.50 kG.[28] This difference might be explained by assuming that the true demagnetizing field inside the sample differs from that obtained by approximating its geometry to an ellipsoid. It probably is a real difference due to the fact that the sample used here has much higher purity than that used for the earlier determination. Since this value is of great importance in determining the band structure of ferromagnetic nickel, new measurements of $4\pi M_s$ should be carried out with samples of high purity.

IV. RESULTS AND DISCUSSIONS

Since nickel has high crystal symmetry, data were taken only with field directions in the $(1\bar{1}0)$ and (100) symmetry planes. The two distinct sets of frequencies F observed with field directed in these two planes were converted to extremal cross-sectional areas by

$$\text{Area (in a.u.)}=2.673\times10^{-9}F \text{ (in G)} \tag{7}$$

and plotted versus magnetic field directions.

The DHVA oscillations can be observed either by varying B while keeping its direction fixed or by varying

[27] E. C. Stoner, Phil. Mag. **36**, 803 (1945).
[28] P. Weiss and R. Forrer, Ann. Phys. (Paris) **12**, 329 (1929).

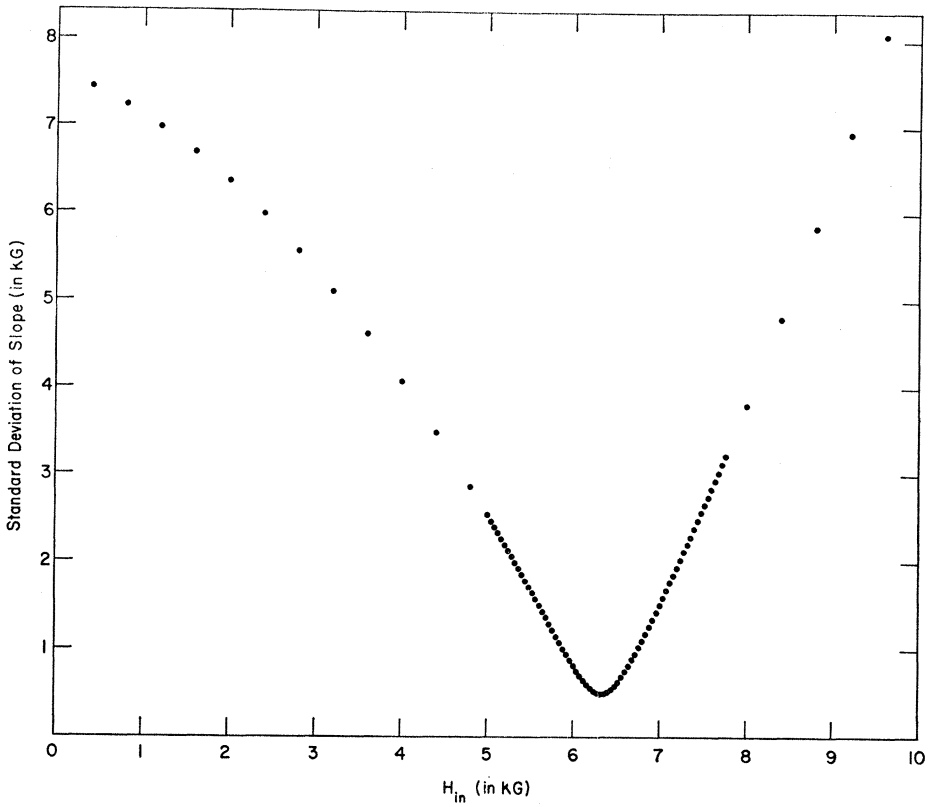

FIG. 8. Standard deviation of slope as a function of the variable parameter H_{in}.

the direction of **B** while its magnitude is kept constant.[29] In the former, one can obtain the absolute value of the DHVA frequency by

$$F=n\times B_0\times B_n/(B_n-B_0), \tag{8}$$

where n is the number of oscillations observed, as B is swept from B_0 to B_n. In the latter, one measures the differential change of the DHVA frequency F as a function of field orientation by

$$F(\theta_1)-F(\theta_2)=mB, \tag{9}$$

where m is the number of oscillations observed as the field orientation is changed from θ_1 to θ_2. Because of the very high phase of the DHVA oscillations ($F\gg B$), the latter method is by far the more accurate one for studying the field-orientation dependence of the DHVA frequencies. Thus the angular variation of each of the area branches was determined by this field-rotation technique. The absolute value of the frequencies was measured to better than 1% and the field directions accurate to to better than 1°.

As discussed in Sec. III, our He^3 refrigerator does not permit accurate measurement of sample temperature, so that no detailed studies on the temperature dependence of the amplitude of the observed DHVA oscillations were carried out to yield effective-mass data. The effective-mass values listed in Table I were measured with the 53-kG superconducting magnet system at

TABLE I. DHVA frequencies and effective masses measured at major symmetry directions.

Fermi surface	Symmetry directions	Extremal area (10^{-2} a.u.)	DHVA frequency (10^6 G)	m^*/m_0
Spin-↑ s-band neck	[111]	0.716	2.68	0.25±0.02
	[110]	1.02	3.84	0.36±0.02
X_5↓ d-band hole pocket	[100]	2.70	10.12	1.0±0.1
		6.65	24.9	1.9±0.2 (at $\theta=7°$)
	[111]	4.22	15.8	...
	[110]	3.79	14.2	1.35±0.1
		5.85	21.9	1.4±0.3

[29] D. Shoenberg and P. J. Stiles, Proc. Roy. Soc. (London) **A281**, 62 (1964).

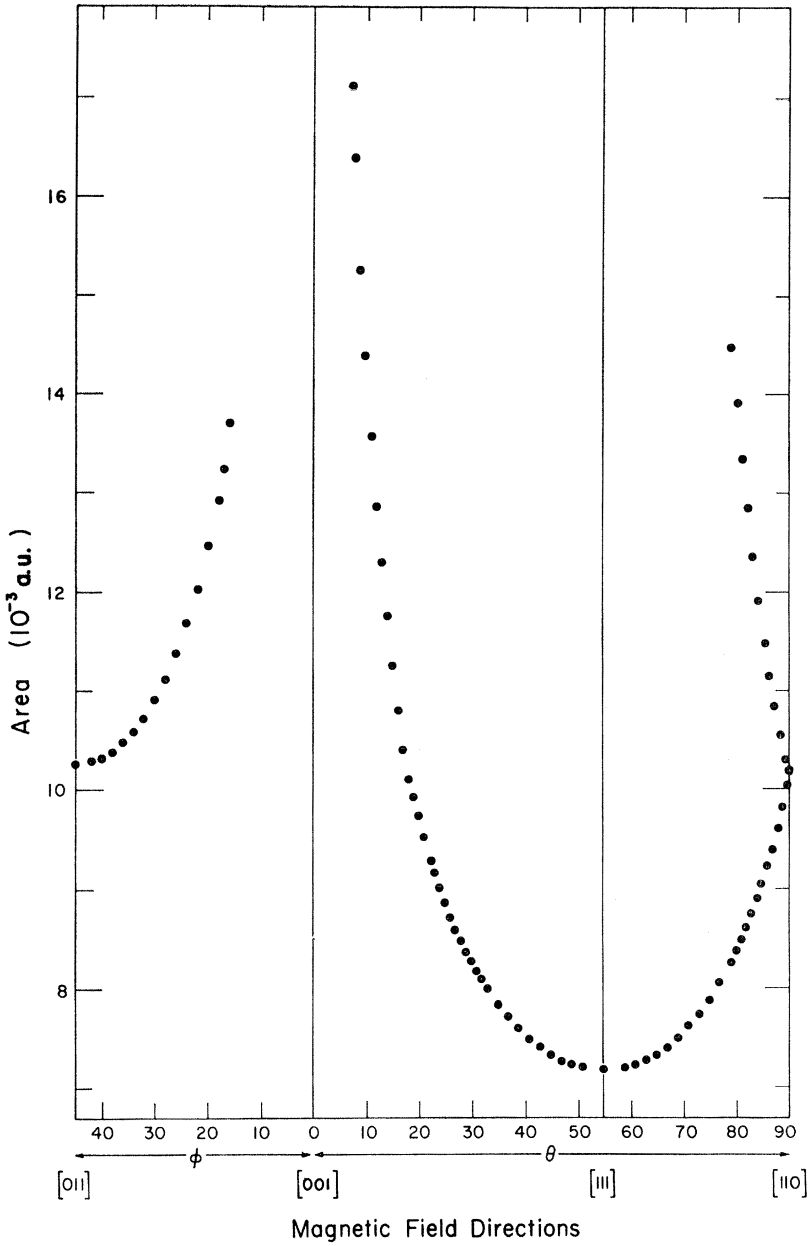

FIG. 9. Angular variation of the DHVA extremal cross-sectional area branches in the (100) and (1$\bar{1}$0) symmetry planes of nickel (for area $<2\times10^{-2}$ a.u.).

He[4] temperatures as described in the preliminary report.[25] We also list in Table I a summary of all the DHVA areas observed in the present investigation for field directions along the major crystallographic axes.

A. Neck of the Spin-↑ *s*-band Electron Sheet of the Fermi Surface

The area branch in the (1$\bar{1}$0) plane in Fig. 9 was previously measured by JT and was assigned to the extremal electron orbits on the L_2' neck of the spin-↑ *s*-band electron sheet centered on Γ. In general, the areas measured in this experiment are about 2% lower than those reported by JT. However, since their internal field was determined to ±0.5 kG, this discrepancy is within experimental errors. We have followed this branch to $\theta=6.5°$ from the [100] axis and 12° beyond the [110] axis. Figure 10 shows a log plot of the DHVA signal amplitude as a function of θ. The drastic reduction in amplitude near $\theta=6.5°$ shows that there is a saddle-point cutoff at $\theta=6.5°$ on this orbit.

The assignment of this area branch to the neck of the spin-↑ electron sheet is consistent with the (100) plane data measured in this experiment. The data in this plane were followed 30° from the [110] axis. When the magnetic field was tilted off the (100) symmetry plane, strong beat structure was observed in the DHVA

oscillations. This beat structure was due to the splitting of the area degeneracy of extremal electron orbits on the [111] and the [$\bar{1}$11] directed necks. This sensitive indicator of small deviations of **H** from the crystal symmetry plane was used to correct small misorientations by tilting the entire cryostat assembly.

For small values of **k**, we can make a hyperbolic expansion for the energy surfaces near L_2':

$$E(k)-E(L_2')=\tfrac{1}{2}\hbar^2[(k_x^2+k_y^2)/m_t-k_z^2/m_l], \quad (10)$$

where k_x, k_y, and k_z are measured from L with the z axis chosen parallel to the [111] axis, and m_l and m_t are the longitudinal and transverse masses relative to the z axis. The angular variation of the extremal cross-sectional area of the Fermi surface is then given by

$$A(\psi)=\frac{A(111)}{\cos\psi[1-(m_t/m_l)\tan^2\psi]^{1/2}}, \quad (11)$$

where the angle ψ is measured from the [111] axis, and $A(111)$ is the minimum area of the branch for H parallel to [111]. For $\psi\leq 20°$, the angular variation of the area branch is symmetric (to within 1%) about [111] in the (1$\bar{1}$0) plane as shown in Fig. 9. For this range of ψ, the experimental data can be represented by Eq. (11) with $m_t/m_l=0.38\pm0.01$.

If we assume that the experimental effective mass $[m_t^*(111)=0.25\pm0.02]$ provides a good measurement of the actual band-structure mass, the Fermi energy of the neck measured relative to $L_2'\uparrow$ is given by

$$E_f(\text{neck})=E_F-E(L_2')=(\hbar^2/2\pi)[A(111)/m_t^*(111)]. \quad (12)$$

Thus, $E_f(\text{neck})=0.009$ Ry. However, this value must differ from the actual Fermi energy by a scale factor.

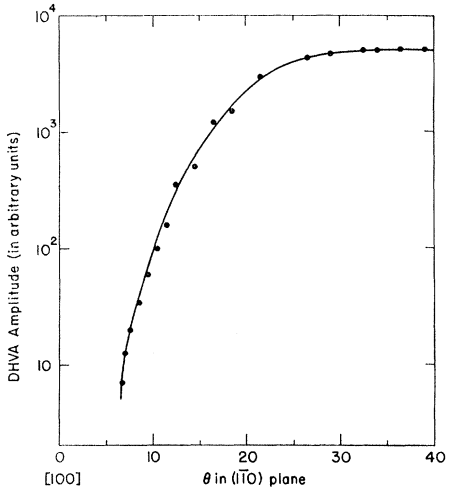

FIG. 10. Decrease of the DHVA amplitude of the neck area branch near a saddle-point cutoff in the (1$\bar{1}$0) plane.

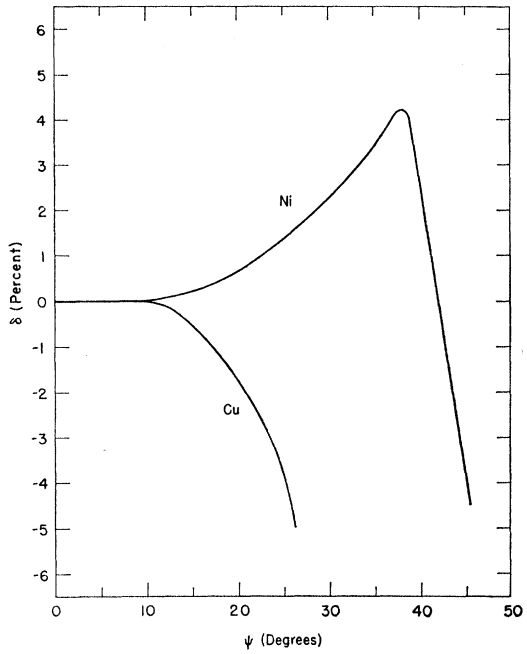

FIG. 11. Asymmetry of the neck area branch about the ⟨111⟩ axis in the (1$\bar{1}$0) plane for Ni and Cu. The data for Cu are taken from Ref. 31.

This scale factor is determined by many-body mass-enhancement effects (electron-electron, electron-phonon, electron-magnon) which we have insufficient experimental information to determine. Phillips[30] estimates that the enhancement scale factor is about 2.8. Thus $E_f(\text{neck})\approx 0.025$ Ry.

The hyperbolic energy surface given by Eq. (10) does not have the appropriate form to satisfy the crystal symmetry about L for large values of k. Therefore, Eq. (11) can not be expected to describe the angular variation of the entire experimental area branches in Fig. 9. Figure 11 shows the asymmetry of the neck data about [111] in the (1$\bar{1}$0) plane. The asymmetry is measured by the parameter δ defined by

$$\delta=[A_2(\psi)-A_1(\psi)]/A_1(\psi), \quad (13)$$

where $A_1(\psi)$ and $A_2(\psi)$ are the extremal areas measured while the magnetic field is in the (1$\bar{1}$0) plane at an angle ψ from the [111] axis in the direction towards [100] and [110], respectively. This small degree of asymmetry was accurately measured by using the field-rotation method discussed above.

Since this spin-$\uparrow$ s-band electron sheet has the same topology as the Fermi surface of copper, which has been extensively studied experimentally, we summarize in Table II the results of copper taken from Joseph

[30] J. C. Phillips, *Proceedings of the International School of Physics, Enrico Fermi, Course XXXVII* (Academic Press Inc., New York, 1967).

TABLE II. Comparison of the DHVA data on the neck of the Fermi surface in Ni with that in Cu taken from Joseph *et al.*[a]

	Nickel	Copper
$A(111)$	0.716×10^{-2} a.u.	5.846×10^{-2} a.u.
m^*/m_0 (111)	0.25	0.46
m_t/m_l	0.38 ± 0.01	2.54
Observable in $(1\bar{1}0)$ plane	from $\theta=6.5°$ to $\theta=102°$	from $\theta=28.9°$ to $\theta=83°$

[a] Reference 31.

et al.[31] The asymmetry of the neck area branch about [111] in the $(1\bar{1}0)$ plane in copper is opposite to that observed in nickel. This is also plotted in Fig. 11.

B. *d*-band Hole Pocket

The complex of area branches labeled by χ_G in Fig. 12 arises from three equivalent closed sheets of Fermi surface. The angular variation of these branches in the (100) and $(1\bar{1}0)$ symmetry planes indicates that they are centered on the symmetry points X of the BZ (Fig. 1). The effective masses (Table I) measured from the temperature dependence of the DHVA amplitude at various points on these branches are larger than that expected from a nearly-free-electron-like sp band. Since the band-structure models predict sheets of the Fermi surface having this general symmetry and size, we can tentatively conclude that they arise from a set of d-band X pockets. These pockets are essentially ellipsoidal. The major axis of each is oriented along the Δ symmetry line passing through the symmetry points X on which it is centered. The subscripts **G** label the direction of the major axis of the particular Fermi-surface sheet associated with the extremal cross-sectional area branch in Fig. 12.

That the Fermi surface deviates from an ellipsoid of revolution is seen by the large anisotropy exhibited by the $\chi_{[100]}$ branch in the (100) plane and the rapid decrease of the $\chi_{[010]}$ and $\chi_{[001]}$ branches as the magnetic field is tilted away from the [001] and [110] axes, respectively. Moreover, when the magnetic field is tilted away from the [001] axis, the $\chi_{[001]}$ branch in both symmetry planes varies more rapidly than that expected from a cylindrical surface oriented along the [001] axis (shown as dashed curves in Fig. 12). This would normally imply that the Fermi surface is dumbbell shaped. However, we did not observe any beat structure in the DHVA oscillations that could indicate the existence of the noncentral extremal orbits expected from a dumbbell surface. Thus, the unusual angular variation of the χ_G branches indicates that the d-band X pockets from which they arise are highly fluted sheets of Fermi surface.

In the preliminary results of the present investigation,[25] data points unrelated to the χ_G branches were observed in a magnetic field range of 5° about $\theta=75°$ in the $(1\bar{1}0)$ plane. Since the present data were taken with samples of much greater crystal perfection, higher purity, better geometry, and at lower temperatures, the signal-to-noise ratio was greatly improved. We were able to follow all the χ_G branches throughout the entire extent of the $(1\bar{1}0)$ and (100) planes by using both rotation-diagram and field-sweep methods. The second harmonic of the $\chi_{[001]}$ branch was observed in both the $(1\bar{1}0)$ and the (100) planes for an angular range of about 30° on either side of [001]. We also observed the second and higher harmonics of the neck branch. We

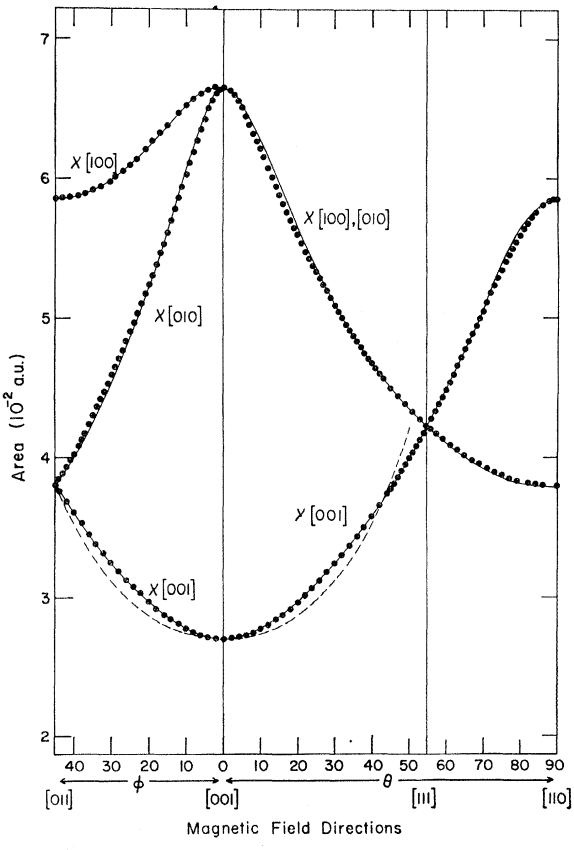

FIG. 12. Angular variation of the DHVA extremal cross-sectional area branches in the (100) and $(1\bar{1}0)$ planes of nickel (for area $>2\times10^{-2}$ a.u.). The solid curves show the corresponding areas for the model Fermi surface represented by Eq. (14). The dashed curve shows the angular variation of the extremal areas of a cylindrical Fermi surface oriented along the ⟨001⟩ axis.

[31] A. S. Joseph, A. C. Thorsen, E. Gertner, and L. E. Valby, Phys. Rev. **148**, 569 (1966).

did not observe any DHVA frequency that was unrelated to the χ_G or the neck area branches. We believe that the isolated data points observed in the preliminary measurements were spurious and were perhaps due to small crystal inclusions.

The solid curves in Fig. 12 show the angular variation of the extremal cross-sectional area of a parameterized-model Fermi surface which was generated in order to allow the conversion of the measured area branches into Fermi-surface radii. The model which is consistent with the symmetry at X is given by

$$k^2=\frac{R_\varphi^2 R_z^2}{R_z^2+(R_\varphi^2-R_z^2)\cos^2\theta}+C_2\cos^2\theta-C_4\cos^4\theta,$$

$$R_\varphi=R_0+R_4\cos 4\varphi+R_8\cos 8\varphi \qquad (14)$$

where k is the length of the $\mathbf{k}$ vector from X to a point

TABLE III. Parameters of the $X_5\downarrow$ hole pocket (in a.u.). The lattice parameter of Ni used in calculating the BZ volume and ΓX ($a=6.643$ a.u.) is from Wyckoff[a] and extrapolated to 1°K using the thermal-expansion data from White.[b]

$R_z=0.213$	
$R_0=9.28\times10^{-2}$	$C_2=6.8\times10^{-3}$
$R_4=6.05\times10^{-3}$	$C_4=9.07\times10^{-3}$
$R_8=6.54\times10^{-4}$	
$k_{X\Gamma}=0.207$	
$k_{XW}=0.099$	$\Gamma X-k_{X\Gamma}=0.739$
$k_{XU}=0.087$	
$n_h=0.0072$ holes/atom	
$E_F(X_5)=0.008\pm0.001$ Ry	

[a] R. W. G. Wickoff, *Crystal Structures* (Interscience Publishers, Inc. New York, 1960).
[b] G. K. White, *Experimental Techniques in Low Temperature Physics* (Oxford University Press, London, 1959), p. 285.

on the Fermi surface specified by the usual spherical coordinates (θ, φ) choosing XW, [100], and $X\Gamma$, [001], as x and z axes, respectively. The values of these parameters were so chosen that the central extremal areas calculated from this model agreed best with the experimentally measured areas in the major symmetry planes shown in Fig. 12. The values, which are listed in Table III together with the resulting Fermi-surface radii measured from X in the three principal crystallographic directions, were used to obtain the solid curves in Fig. 12. The cross sections of this model Fermi surface in the major symmetry planes are shown in Fig. 13.

Note that by setting $R_4=R_8=C_2=C_4=0$, Eq. (14) represents an ellipsoid of revolution about the z axis. The fluted character of the model, as seen in Fig. 13, is required to fit the unusual angular variation of the χ_G data branches discussed above. In Fig. 14, the cross-sectional area $A(k_z)$ of this model is plotted as a function of k_z. Here, k_z is the projection on the $X\Gamma$ line of the $\mathbf{k}$ vector measured from X, and $A(k_z)$ is the cross-

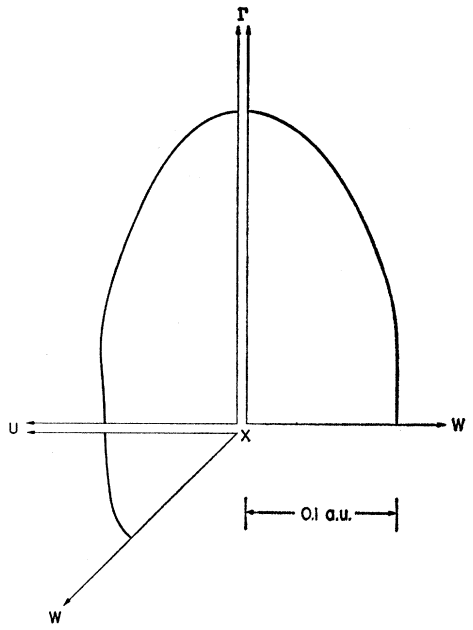

FIG. 13. Cross sections of the model Fermi surface represented by Eq. (14) in major symmetry planes.

sectional area of the model Fermi surface at k_z in the plane normal to the $X\Gamma$ line. Figure 14 shows that this model surface is slightly dumbbell shaped and has an extra extremal area which is about 4% larger than the central extremal area. As mentioned previously, we did not observe any beat structure in the DHVA oscillations of the $\chi_{[001]}$ branch which could indicate an extra non-central extremal area on the Fermi surface. This, together with the fact that this model fits the experimental data to better than 1.5%, implies that the present data which are limited in the (100) and (1$\bar{1}$0) symmetry planes are not sufficient to determine uniquely the

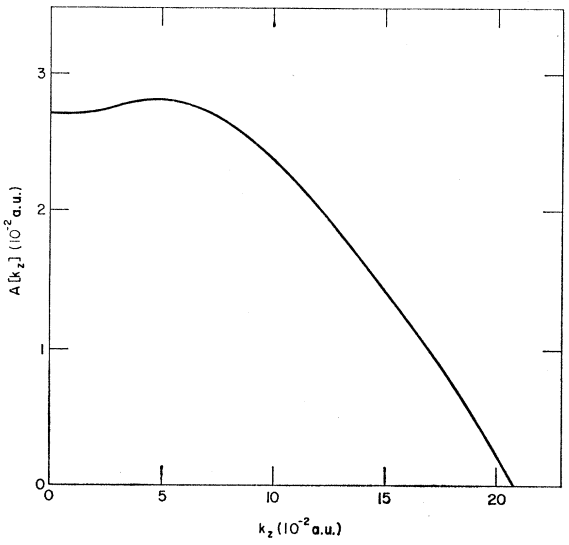

FIG. 14. Cross-sectional area $A(k_z)$ of the model surface normal to the z axis as a function of k_z.

geometry of the Fermi surface. This sheet of Fermi surface is apparently more fluted than that pictured in Fig. 13. The Fermi-surface radii given by Eq. (14) can, therefore, be in error by as much as 2%.

If we assume that the measured effective mass is the correct band-structure mass, the Fermi energy of this pocket, estimated from a parabolic band model, is 0.008 Ry. The many-body mass-enhancement effects will probably increase this energy somewhat. The 2% uncertainty in the Fermi-surface radii can be expected to introduce an uncertainty in the over-all band energy of about 5×10^{-4} Ry. This energy uncertainty is beyond the accuracy of any first-principles band-structure calculations even in simple metals.

The schematic band structure shown in Fig. 3 is representative of the models recently proposed. Either the $X_2\downarrow$ or the $X_5\downarrow$ d-band hole pocket[32] of this model has the symmetry appropriate to fit the χ_G branches in Fig. 12. However, the $X_2\downarrow$ energy band is flatter than the $X_5\downarrow$ energy band and consequently the $X_2\downarrow$ pocket should have larger effective mass than the $X_5\downarrow$ pocket. Thus, if the cross-sectional areas of these two pockets were about the same size, the χ_G frequency branches should arise from the $X_5\downarrow$ pocket.

No evidence for another X-centered pocket was obtained in the present DHVA investigation. When the magnetic field **H** was along the [001] axis, the signal-to-noise ratio was large enough to allow the detection of another frequency branch having amplitude as small as 0.002 times the amplitude of the $\chi_{[001]}$ branch. Also for this magnetic field direction, the DHVA oscillations from the $\chi_{[001]}$ branch were observed for H as small as 11 kG. This implies that the inhomogeneity in the **B** field was less than 30 G over the sample. This field inhomogeneity should result primarily from the sample geometry and should be field-independent. If there were magnetic domains existing in the sample which were responsible for part of this inhomogeneity, then this **B**-field inhomogeneity should decrease at higher **H** field. In any case, this B-field inhomogeneity should allow the observation of DHVA frequencies at least six times higher than that of the $\chi_{[001]}$ branch when H was 37 kG. Therefore, if an $X_2\downarrow$ pocket existed comparable in size to the $X_5\downarrow$ pocket, the fact that we did not observe the DHVA effect at 0.3°K implies that its effective masses had to be at least seven times as large as those of the $X_5\downarrow$ pocket. On the other hand, if the $X_2\downarrow$ pocket existed and had effective masses twice as large as those of the $X_5\downarrow$ pocket, we should have observed its DHVA oscillations even if its extremal cross-sectional area in the plane normal to [001] should be *five times larger* than that of the $X_5\downarrow$ pocket.

[32] Strictly speaking, the irreducible representations X_5 and X_2 label the bands at the symmetry point X only. We use them rather loosely here to designate the bands about X which have irreducible representations along symmetry lines compatible with X_5 and X_2.

If the $X_2\downarrow$ and $X_5\downarrow$ levels crossed above the Fermi level E_F for *some* directions from X but *not for all* directions, as shown in Fig. 15, the resulting sheets of Fermi surface would not have purely $X_2\downarrow$ or $X_5\downarrow$ character. Instead, two sets of pockets would exist, each having some regions from the heavy-mass $X_2\downarrow$ level with the remaining regions coming from the light-mass $X_5\downarrow$ level. For the cases shown in Figs. 15(a) and 15(b), this would be expected to result in a highly anisotropic variation of the effective cyclotron mass. Within experimental error, this was not observed in the effective-mass data listed in Table I. In addition, when **H** is along the [001] axis, the extremal electron orbits on both pockets would be composed of regions from both the $X_2\downarrow$ and $X_5\downarrow$ levels. Consequently, both the extremal areas and the effective masses of these two pockets would be comparable and we should have observed DHVA oscillations from both pockets near the [001] axis. For the case of the crossing shown in Fig. 15(c), we would have to assign the $\chi_{[001]}$ data branch observed near [001] to the light-mass band whose polar regions are from the $X_2\downarrow$ level. If this were the appropriate case, we should have observed the heavy-mass band near [001] if the pocket size and effective mass satisfied the experimental criteria listed previously for the observation of a pure $X_2\downarrow$ pocket. In all of these cases of band crossings, with the possible exception of that shown in Fig. 15(c), we should have observed two distinct sets of DHVA area branches. Thus, the χ_G branches almost certainly arise from a pure $X_5\downarrow$ pocket.

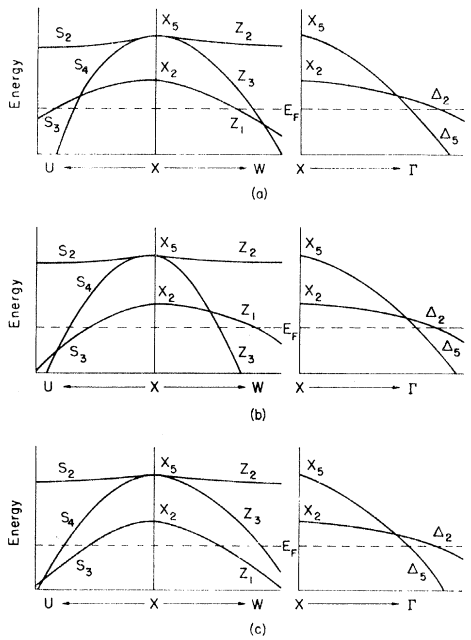

FIG. 15. Schematic drawings of the spin-$\downarrow$ energy bands (near E_F) about X showing that the $X_2\downarrow$ and $X_5\downarrow$ bands crossed above E_F for some directions from X but not all. These three cases are compatable with the magnetic breakdown effect discussed in the text.

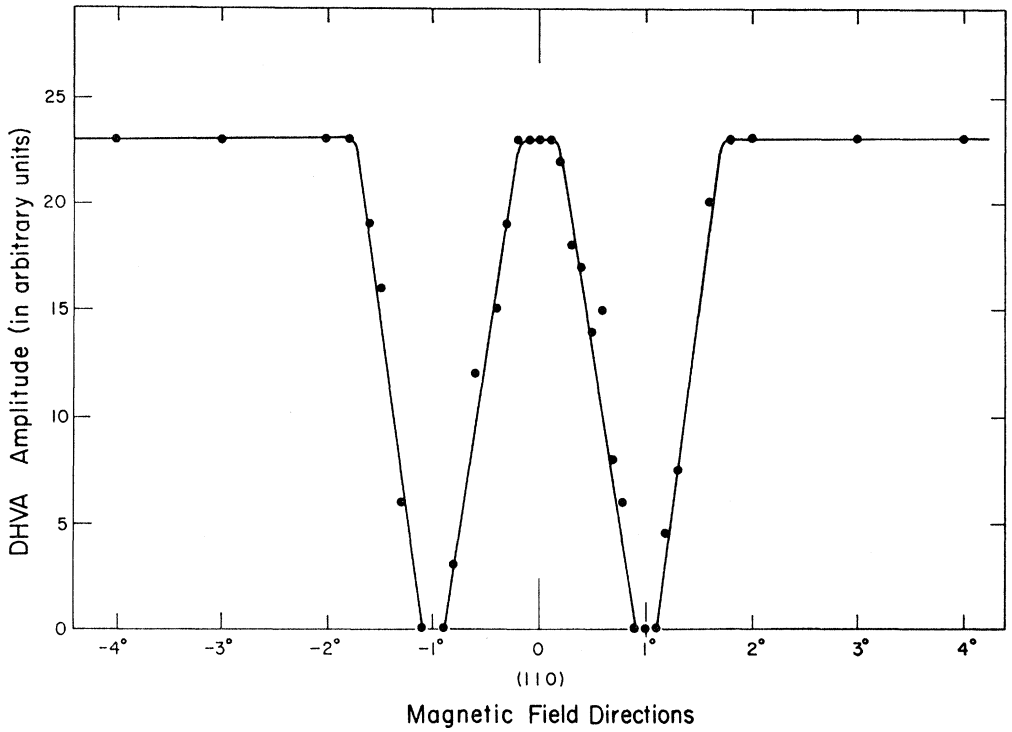

FIG. 16. DHVA amplitude of the $\chi_{[001]}$ branch near the $\langle 110\rangle$ axis in the $(1\bar{1}0)$ plane.

Without spin-orbit coupling, the $X_5\downarrow$ level is doubly degenerate along the $X\Gamma$ symmetry line. The $X_5\downarrow$ pocket and the 5th band electron sheet centered on Γ have a small area of contact around the $X\Gamma$ symmetry line. This degeneracy is removed by the spin-orbit coupling energy gap which is expected to be small enough to allow magnetic breakdown in fields of the order of 30 kG from the $X_5\downarrow$ pocket to the 5th band electron sheet near the $X\Gamma$ line. This effect should be seen as a decrease in the amplitude of the DHVA signal when the extremal electron orbit approaches the $X\Gamma$ symmetry line.

Figure 16 shows the amplitude of the $\chi_{[001]}$ DHVA branch versus magnetic field direction near the [110] axis in the $(1\bar{1}0)$ plane. As the field direction comes close to the [110] axis, the extremal electron orbit which gives rise to the DHVA signal approaches the $X\Gamma$ symmetry line. The sudden decrease observed in the DHVA signal amplitude when the field direction is about 1° from the [110] axis may be due to this magnetic breakdown effect. The fact that the DHVA amplitude actually goes to zero for 0.2° and then regains its previous amplitude seems to indicate a band degeneracy at this point that is not removed by spin-orbit effects. This thus tends to support our previous contention that the χ_G area branches shown in Fig. 12 arise from the $X_5\downarrow$ pocket. The rise of the DHVA amplitude back to its original value when the field is oriented along the [110] axis indicates that the spin-orbit gap along $X\Gamma$ is considerably larger than the total gap existing slightly off $X\Gamma$. Thus it appears that the $X_5\downarrow$ pocket and the 5th-band electron sheet are degenerate at four points near $X\Gamma$ at an angle of 1.5° from the $X\Gamma$ symmetry line measured from X toward W. This unusual geometry is puzzling but perhaps understandable, since the spin-orbit coupling is expected to be the strongest along the symmetry line. In any case, this amplitude behavior would be completely incomprehensible if the extremal electron orbits were on an $X_2\downarrow$ level in this region.[33]

V. CONCLUSIONS

Two distinct sets of DHVA-frequency branches were observed in this investigation. The lower-frequency set

[33] *Note added in proof.* The recent work of L. Hodges, D. R. Stone, and A. V. Gold [Phys. Rev. Letters, **19**, 655 (1967)] interprets the asymmetry of this hole pocket in terms of the *d-s-p* band model Hamiltonian discussed in Ref. 15 but changed to include the effects of spin-orbit interactions. They were able, with this additional parameterization, to fit the extremal area variation in the major symmetry planes and also were able with this model to eliminate the second extrema for **H** along [001]. The geometric model discussed above is just the $\mathbf{k}\cdot\mathbf{p}$ perturbation expansion expressed in trigonometric functions; the expansion was carried out to the highest order that was warranted by the experimental data. A unique determination of the coefficients of higher order terms in this expansion cannot be made without recourse to additional data taken in nonsymmetry planes of the crystal. The single additional spin-orbit parameter introduced by Hodges *et al.* seems to be successful in accounting for all of the area data. In addition, the field-dependent band structure which results from their calculation makes the puzzling amplitude variation shown in Fig. 16 much more understandable.

extends the spin-$\uparrow$ s-band neck data previously measured by JT. We obtained no evidence for a neck comparable in size on the spin-$\downarrow$ d-band sheet, as suggested in Ref. 13. The higher-frequency set of DHVA branches was shown to be from a set of purely $X_5\downarrow$ hole pockets. These pockets are fluted ellipsoids containing a total of 0.0073 holes/atom. Since the $X_1\downarrow$ pocket and the 5th-band electron sheet are nearly degenerate along Δ, the major axis of the $X_5\downarrow$ pocket also gives the ΓX linear dimension of the large d-band surface centered on Γ ($\Gamma X - k_{X\Gamma} = 0.739$ a.u. in Table III). We did not observe any DHVA oscillations which could be assigned to either the $X_2\downarrow$ or the $L_3\downarrow$ pockets. Since the signal-to-noise ratio for detecting the χ_G branches is large, the fact that we did not detect any DHVA effect from these hole pockets at 0.3°K makes their existence doubtful.

Thus, from the data we can deduce several details about the structure of the spin-$\downarrow$ d bands near E_F. None of the model band-structure calculations that have appeared in the literature agree quantitatively with these experimental results. However, the general qualitative features of all these models are compatible with the DHVA effect observed in this experiment. They all require a set of X-centered hole pockets in the spin-$\downarrow$ d bands similar to those measured in this experiment. All of these model band-structure calculations are based on the same general approximation: The ferromagnetic energy bands are obtained by treating the many-body interactions responsible for ferromagnetism as a perturbation on the one-electron band structure for nickel in its hypothetical nonmagnetic state. These many-body effects are assumed to have some plausible simple form and are then determined (generally semiempirically) to yield a ferromagnetic band structure that agrees at least qualitatively with the limited experimental data. Therefore, we cannot expect these models to yield detailed quantitative agreement with our experimental data. On the other hand, the fact that the general features of their spin-$\downarrow$ d bands are in qualitative agreement with the data is direct experimental confirmation of this general theoretical approach to the ferromagnetic electronic band structure of nickel.

Our data are insufficient to yield detailed information about the many-body interactions which are responsible for ferromagnetism in nickel. An accurate ferromagnetic band structure can probably only be obtained semiempirically when complete DHVA data are obtained. This, of course, will require further DHVA investigation in much higher fields and probably with even purer samples.

ACKNOWLEDGMENTS

I would like to record my gratitude to Professor R. W. Stark for his keen interest, patient guidance, and encouragement during all phases of this work. I have benefited greatly from discussions with J. C. Kimball, F. M. Mueller, and E. I. Zornberg.

APPENDIX

When the magnitude of the applied field $\mathbf{H}$ is modulated by $H_m\cos\omega t$, the $\mathbf{B}$ field inside the sample is given by

$$\begin{aligned}\mathbf{B}&=(H+H_{\rm in}+H_m\cos\omega t)\hat{H}\\&=(B_0+H_m\cos\omega t)\hat{H},\\B_0&=H+H_{\rm in},\end{aligned}$$

where $\hat{H}$ is a unit vector along $\mathbf{H}$, H_m is the amplitude of the modulation field with frequency ω, and B_0 is the magnetic induction used in calculating the DHVA frequencies. In this experiment, $H_m/B_0 \lesssim 10^{-2}$. The DHVA magnetization having frequency F_i is then given by

$$\mathbf{M}_i(\mathbf{B})=\boldsymbol{\alpha}_i(\mathbf{B})\ \mathrm{Im}\{\exp[i(2\pi F_i/B_0+H_m\cos\omega t+\beta_i)]\}.$$

To first order in H_m/B_0, we can ignore the time dependence of $\boldsymbol{\alpha}_i$ and write $\mathbf{M}_i(\mathbf{B})$ as

$$\mathbf{M}_i(\mathbf{B})\simeq\boldsymbol{\alpha}_i(\mathbf{B}_0)\ \mathrm{Im}\left(\exp\{i[2\pi F_i/B_0(1-H_m\cos\omega t/B_0)+\beta_i]\}\right)=\boldsymbol{\alpha}_i(\mathbf{B}_0)\ \mathrm{Im}\{\exp[i(2\pi F_i/B_0+\beta_i)]\exp(-iX\cos\omega t)\},$$

where

$$X=2\pi F_iH_m/B_0^2. \tag{A1}$$

We can obtain the harmonic content of $\mathbf{M}_i(\mathbf{B})$ by Fourier analysis of $\exp(-iX\cos\omega t)$:

$$\exp(-iX\cos\omega t)=\sum_{-\infty}^{\infty}J_n(X)i^n\exp(-in\omega t)=J_0(X)+\sum_{n=1}^{\infty}i^n2J_n(X)\cos n\omega t.$$

Hence

$$\begin{aligned}\mathbf{M}_i(\mathbf{B})&\simeq\boldsymbol{\alpha}_i(\mathbf{B}_0)\ \mathrm{Im}\{\exp[i(2\pi F_i/B_0+\beta_i)][J_0(X)+\sum_{n=1}^{\infty}i^n2J_n(X)\cos n\omega t]\}\\&=\boldsymbol{\alpha}_i(\mathbf{B}_0)\{\sin(2\pi F_i/B_0+\beta_i)J_0(X)+\sum_{n=1}^{\infty}[\sin(2\pi F_i/B_0+\beta_i+\tfrac{1}{2}(n\pi))]2J_n(X)\cos n\omega t\}.\end{aligned} \tag{A2}$$

The induced emf on the pickup coil due to the DHVA magnetization of frequency F_i is given by

$$\text{emf}_i = d/dt[\mathbf{M}_i(\mathbf{B})\cdot\hat{\mu}] \simeq -\hat{\mu}\cdot\boldsymbol{\alpha}_i(\mathbf{B}_0)\sum_{n=1}^{\infty}[\sin(2\pi F_i/B_0+\beta_i+\tfrac{1}{2}(n\pi))]J_n(X)2n\omega\sin n\omega t, \tag{A3}$$

where $\hat{\mu}$ is a unit vector along the pickup coil axis and X is defined by

$$X = 2\pi F_i H_m/B_0^2.$$

PHYSICAL REVIEW VOLUME 164, NUMBER 2 10 DECEMBER 1967

Specific-Heat Anomaly and Calculation of the Configurational Entropy Change at the Phase Transition in Copper Formate Tetrahydrate*

KENKICHI OKADA
Nagoya Institute of Technology, Gokiso-cho, Showa-ku, Nagoya, Japan

(Received 4 May 1967)

Specific-heat anomalies of copper formate tetrahydrate, $Cu(HCOO)_2 4H_2O$, and its deuterium substitute $Cu(HCOO)_2 4D_2O$ were found at respective antiferroelectric transition points. It has a typical λ shape, sharply peaked at the transition. The transition point was shifted from -37.7 to -27.5°C by deuterium substitution. The transition entropies were measured as 0.78 and 0.90 cal/mole deg in hydrated and deutrated crystals, respectively. The transition was considered to be due to an order-disorder phenomenon arising from the hydrogens in the water of crystallization. The number of configurations of hydrogens in the water layer of the structure, the positions of which have been determined by a previous neutron-diffraction study at room temperature, was calculated taking account of the full correlation through oxygens by the use of a simple equivalent model. A different value was obtained from that obtained by Pauling's method; the latter does not agree with experiment in this layer-structured crystal. The configurational entropy change between the disordered and the antiferroelectric states was calculated as $R\ln\frac{1}{2}(2+\sqrt{2})\simeq 1.06$ cal/mole deg. The theoretical value agrees well with the experimental values obtained from thermal measurements on both crystals.

I. INTRODUCTION

COPPER formate tetrahydrate, $Cu(HCOO)_2 4H_2O$, has been investigated extensively because of its magnetic properties at low temperatures. On the other hand, in 1962 Kiriyama[1] reported a dielectric anomaly in this crystal at -36°C, and a mechanism of the anomaly was proposed. The crystal structure, including copper, carbon, and oxygen positions, was determined by Kiriyama *et al.*,[2] who found the crystal to be monoclinic, space group $P2_1/a$ with $a=8.18$, $b=8.15$, $c=6.35$ Å, and $\beta=101°5'$, and with two formula units per unit cell. A neutron-diffraction study[3] was performed in order to obtain the positions of the hydrogens in the water of crystallization at room temperature. During this study some hydrogens were found to be disordered. This stimulated us to measure dielectric properties in detail, and the dielectric anomaly mentioned above was actually found to be due to an antiferroelectric phase transition.[4]

As determined by Kiriyama *et al.*,[2] this crystal has a structure consisting of alternating layers of waters and copper formate groups in the (001) plane. Mookherji and Mathur[5] predicted a two-dimensional antiferromagnetism at low temperature, because of its layer structure. In a similar fashion, a two-dimensional ordering of hydrogens in the water layer which may correspond to the antiferroelectric phase can be expected. As a matter of fact, the neutron-diffraction study[3] showed that the disordered hydrogens are only in the water layer, while the hydrogens bonding water oxygens to formate oxygens are ordered at room temperature. It is plausible that the disordered hydrogens are ordered below the transition point. This order-disorder transition may give an excess entropy detectable by thermal measurements.

The configurational entropy of the order-disorder transition due to hydrogen may be calculated by

* Work supported in part by a grant-in-aid for scientific research from the Ministry of Education, Japan.

[1] H. Kiriyama, Bull. Chem. Soc. Japan **35**, 1199 (1962).
[2] R. Kiriyama, H. Ibamoto, and K. Matsuo, Acta Cryst. **7**, 482 (1954).
[3] K. Okada, M. I. Kay, D. T. Cromer, and I. Almodovar, J. Chem. Phys. **44**, 1648 (1966).
[4] K. Okada, Phys. Rev. Letters **15**, 252 (1965).
[5] A. Mookherji and S. C. Mathur, J. Phys. Chem. Solids **24**, 1386 (1963).